Electron transfer by domain movement in cytochrome bc_1

Zhaolei Zhang*†, Lishar Huang*‡, Vladimir M. Shulmeister§, Young-In Chi‡, Kyeong Kyu Kim‡, Li-Wei Hung†, Antony R. Crofts‖, Edward A. Berry‡ & Sung-Hou Kim*†‡

** E. O. Lawrence Berkeley National Laboratory, † the Graduate Group of Biophysics, and ‡ Department of Chemistry University of California, Berkeley, California, 94720 USA*

‖ Center for Biophysics and Computational Biology, University of Illinois at Urbana-Champaign, Illinois, 61801 USA

§ This paper is dedicated to the memory of our friend and colleague Vladimir M. Shulmeister, a key member on the project until his untimely death on 27 September 1995.

The cytochrome bc_1 is one of the three major respiratory enzyme complexes residing in the inner mitochondrial membrane. Cytochrome bc_1 transfers electrons from ubiquinol to cytochrome *c* and uses the energy thus released to form an electrochemical gradient across the inner membrane. Our X-ray crystal structures of the complex from chicken, cow and rabbit in both the presence and absence of inhibitors of quinone oxidation, reveal two different locations for the extrinsic domain of one component of the enzyme, an iron–sulphur protein. One location is close enough to the supposed quinol oxidation site to allow reduction of the Fe–S protein by ubiquinol. The other site is close enough to cytochrome c_1 to allow oxidation of the Fe–S protein by the cytochrome. As neither location will allow both reactions to proceed at a suitable rate, the reaction mechanism must involve movement of the extrinsic domain of the Fe–S component in order to shuttle electrons from ubiquinol to cytochrome c_1. Such a mechanism has not previously been observed in redox protein complexes.

Energy conversion in the biosphere occurs mainly through respiration and photosynthesis, and represents a flux several orders of magnitude greater than all anthropogenic energy usage. The underlying mechanism involves coupling electron transfer, along a chain of redox or photoredox enzymes, to proton translocation across an organellar membrane in which those redox components are embedded. This gives rise to a transmembrane electrochemical proton gradient, which can be coupled to energy-requiring processes, including synthesis of ATP—a principle first proposed by Mitchell in his chemiosmotic hypothesis[1].

The central component of the electron-transfer chain in mitochondria and in many aerobic or photosynthetic bacteria is a complex of membrane proteins known as the cytochrome bc_1 complex, or ubiquinol:cytochrome *c* oxidoreductase (E.C. 1.10.2.2). This enzyme complex catalyses electron transfer from ubiquinol to a soluble cytochrome *c*; this transfer is coupled to translocation of two protons across the inner mitochondrial membrane per quinol oxidized[2–4]. The complex isolated from beef heart consists of 11 different polypeptides[5,6] and has a relative molecular mass (M_r) of 240K (Table 1). There are four redox centres, namely, two haem groups, b_H and b_L, of cytochrome *b*, one haem group in cytochrome c_1, and one iron–sulphur cluster of the Rieske protein. A mechanism accounting quantitatively for the proton translocation coupled to electron transport by this enzyme is a version of the 'proton-motive Q cycle' of Mitchell[3,4]. The mechanism also explains the pattern of inhibition by the ubiquinone analogues antimycin, stigmatellin, undecylhydroxydiazo benzothiazole, myxothiazol, and methoxyacrylo-stilbene, which bind specifically at one or the other of the two catalytic sites at which quinone is processed[3,4].

Until recently, only a low-resolution structure for the cytochrome bc_1 complex from *Neurospora crassa* was available, from electron microscopy of two-dimensional crystals[7]. More recently, the bc_1 complex from beef mitochondria has been crystallized in three dimensions in a tetragonal space group[8] and in other space groups[9,10]. A partial structure of the complex has been reported from the tetragonal crystals[11,12]. In this structure, the extrinsic domain of the Rieske protein was too disordered to be traced, and cytochrome c_1 was only partially traced.

We have obtained other crystal forms[13] from other species, including one from chicken heart mitochondria that diffracts to 3.0 Å resolution. With these crystals we have now determined the structure of the complex, which includes the functionally important Rieske iron–sulphur protein and cytochrome c_1. We were also able to assign three additional subunits (subunits 8, 10 and 11) that were not assigned before[12].

A comparison of our structures in the presence and absence of various inhibitors shows that the extrinsic domain of the Rieske protein containing the iron–sulphur cluster assumes one of two conformations in the complexes. In one conformation, the iron–sulphur cluster is close to its electron acceptor, the haem group of cytochrome c_1, but far from the presumed binding site of its electron donor, ubiquinol, in cytochrome *b*. In the other conformation, the iron–sulphur cluster is closer to cytochrome *b*, and farther from cytochrome c_1. This conformation is similar to that found in the tetragonal beef crystals[12].

We have located the binding sites for two Q_o-site inhibitors, stigmatellin and myxothiazol, and for the Q_i-site inhibitor, antimycin. The two Q_o-site inhibitors bind in overlapping but not identical sites.

These two conformations for the iron–sulphur protein and three positions for binding of ubiquinone analogue inhibitors are compatible with all the reactions proposed by the Q-cycle mechanism

Table 1 Subunits of the bovine heart cytochrome bc_1 complex

Subunit	Residues	$M_{(r)}$
1 Core 1	446	49,132
2 Core 2	439	46,471
3 Cytochrome *b*	379	42,592
4 Cytochrome c_1	241	27,288
5 Rieske Fe-S	196	21,611
6 13.4K	110	13,347
7 'Q-binding'	81	9,590
8 c_1 'hinge'	78	9,170
9 Fe-S presequence	78	7,956
10 c_1-associated	62	7,198
11 6.4K	56	6,363
Apo-bc_1	2,166	240,718
Fe_2S_2		76
Haem c_1		616
Haem b_H		616
Haem b_L		616
Prosthetic groups		2,014
Holo-bc_1 complex		242,742

for electron transfer coupled to proton translocation. However, no one structure alone would be competent. We therefore propose that the reaction mechanism for electron transfer in the cytochrome bc_1 complex requires a dramatic conformational change involving movement of the iron–sulphur protein.

A preliminary report of these results has appeared in the proceedings of a meeting[14].

Overall shape of cytochrome bc_1 complex dimer

In all crystals of the bc_1 complex from three sources, the complex is

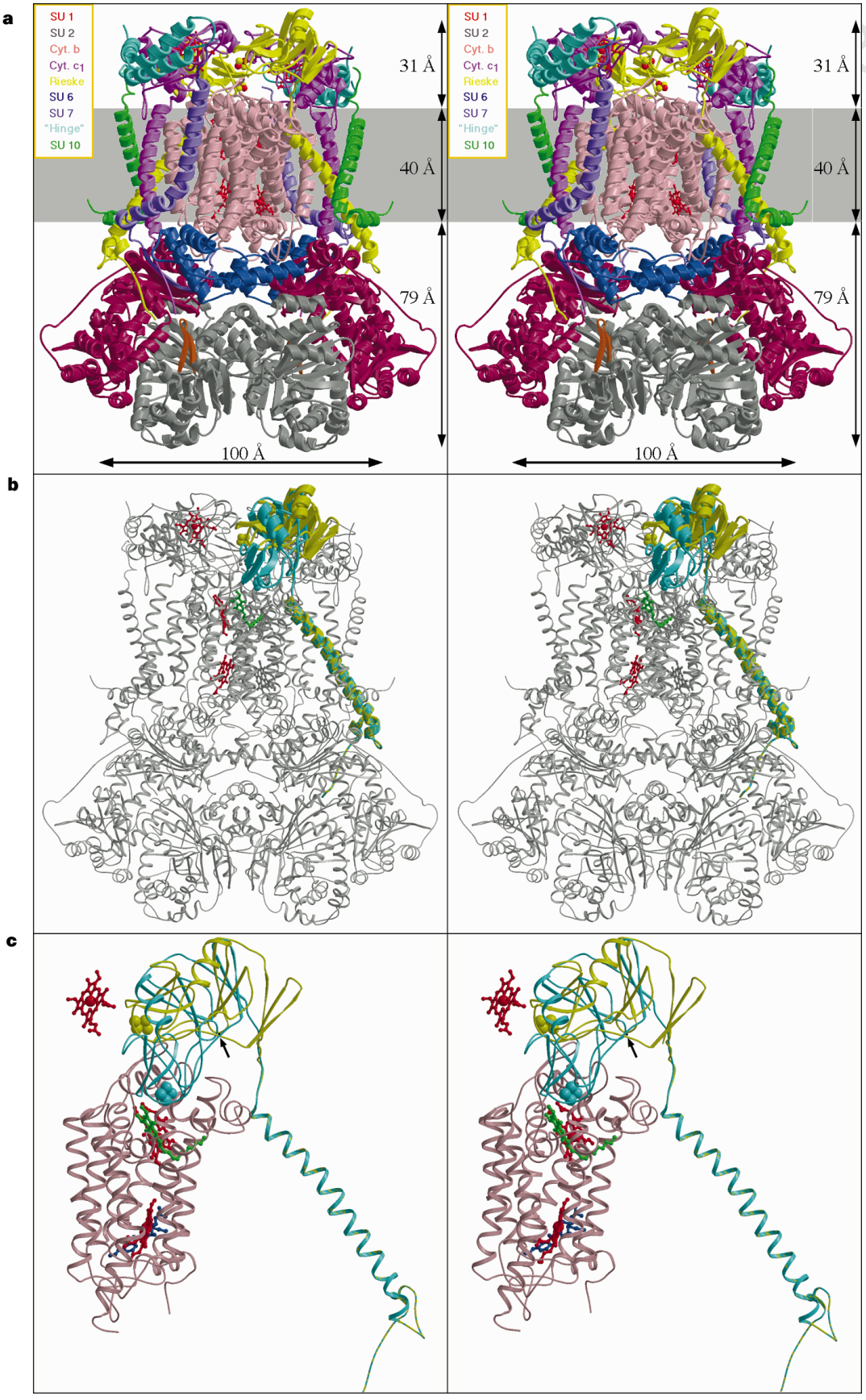

Figure 1 Stereo-view ribbon diagrams of the bc_1 complex. **a**, The native chicken bc_1 dimer. The molecular two-fold axis runs vertically between the two monomers. The key for the colour coding of each subunit is given in the inset. Quinones, phospholipids and detergent molecules are not shown for clarity. The presumed membrane bilayer is represented by a grey band. **b**, Two conformations of the Rieske protein in one monomer shown in the context of the entire dimer. One conformation found in our native chicken crystal (yellow) is superimposed on the other conformation (blue) from crystals grown in the presence of stigmatellin (green stick model). The haem groups (red) of cytochrome c_1 and cytochrome *b* as well as two positions of the iron–sulphur cluster (orange and green balls) of the Rieske protein are shown. **c**, Isolated close-up view of the two conformations of the Rieske protein in contact with cytochrome *b* (pink), with associated haem groups (red), stigmatellin (green) and antimycin (purple). The isolated haem of cytochrome c_1 (red, above) is also shown. SU, subunit; cyt, cytochrome.

present as a dimer (Fig. 1a), in which two monomers are related by a two-fold axis running vertically in the plane of the paper. The protein extends from the membrane 79 Å into the matrix space and 31 Å into the intermembrane region on either side of a transmembrane region 40 Å thick, giving a total length of 150 Å perpendicular to the membrane.

The overall shape of the dimer is similar to that described for the beef complex[11,2], but we have modelled more protein in the intermembrane region. We have located subunits 1–8 and 10 in the electron density of the chicken crystal. We assign subunit 10 to the transmembrane helix labelled N1 in ref. 12, on the basis of good correlation between side chains in the chicken electron density and the beef subunit sequence. Subunit 11 seems not to be present in our preparation of the chicken enzyme, but is present in the beef and rabbit enzymes. It probably corresponds to the transmembrane helix labelled N2 in ref. 12, because this helix is present in the three crystal forms from the beef and rabbit enzymes and not in the chicken crystals.

Subunit 9 has not been assigned yet, and is also missing from the structure of ref. 12. This subunit is the presequence[15] of the Rieske protein, and is cleaved off by a matrix-located processing protease. We also see densities at several sites in the transmembrane portion. We attribute these densities to ubiquinone, detergents and phospholipids.

In the transmembrane domain the helices of the dimer fall into two clearly separated, packed bundles. We have arbitrarily divided the dimer so that one monomer corresponds to one packed bundle of helices in the transmembrane region.

Inhibitor-binding sites

The presence of stoichiometric excesses of the inhibitors antimycin, myxothiazol, or stigmatellin during crystallization resulted in electron-density increases that could be interpreted as being due to the bound inhibitors. The general positions of the antimycin-, stigmatellin- and myxothiazol-binding sites are similar to those inferred from figures in refs 11, 12. Although the limited resolution does not allow the building of detailed atomic models, we have constructed speculative models consistent with the electron density. These inhibitor-binding sites, and especially the Q_o site, are the targets of drug-design efforts to produce environmentally safe and effective plant-protection fungicides for agriculture use[16–18].

The antimycin site. On the basis of its mode of inhibition, antimycin is thought to bind at the Q_i site postulated in the Q-cycle mechanism. At this site, ubiquinone is reduced by electrons from cytochrome *b* accompanied by uptake of protons from the matrix space (resulting in proton translocation when ubiquinol is subsequently oxidized at the Q_o site, with proton release to the external medium). The antimycin-binding site (Fig. 2a) is near the high-potential haem group of cytochrome *b* (b_H), in a cavity surrounded by the haem, the transmembrane helices A, D and E, and the amphipathic surface helix a (secondary structure is defined in Fig. 2c). There may be protonic connection to the matrix phase through or around conserved histidine 202. The close approach of the aromatic ring of the inhibitor to the haem group was expected from the effect of antimycin on the alpha absorption peak of b_H and the fluorescence quenching of antimycin when specifically bound at this site[19]. Residues F221 and T194 are also close enough to contact the inhibitor. One of the haem propionates is in van der Waals contact with the inhibitor and curves around to form an ion pair with R101. The conformation of this propionate, which differs from that depicted for the tetragonal beef crystals[12], is the same in the absence of antimycin.

The stigmatellin site. The stigmatellin-binding pocket (Fig. 2b) is formed by the carboxy-terminal end of helix C, the helix cd1, the ef linker (including the highly conserved sequence PEWY and the helix ef), and the amino-terminal end of helix F. Residues P271, F275, and M125 of cytochrome *b* and H161 of the Rieske protein, which has

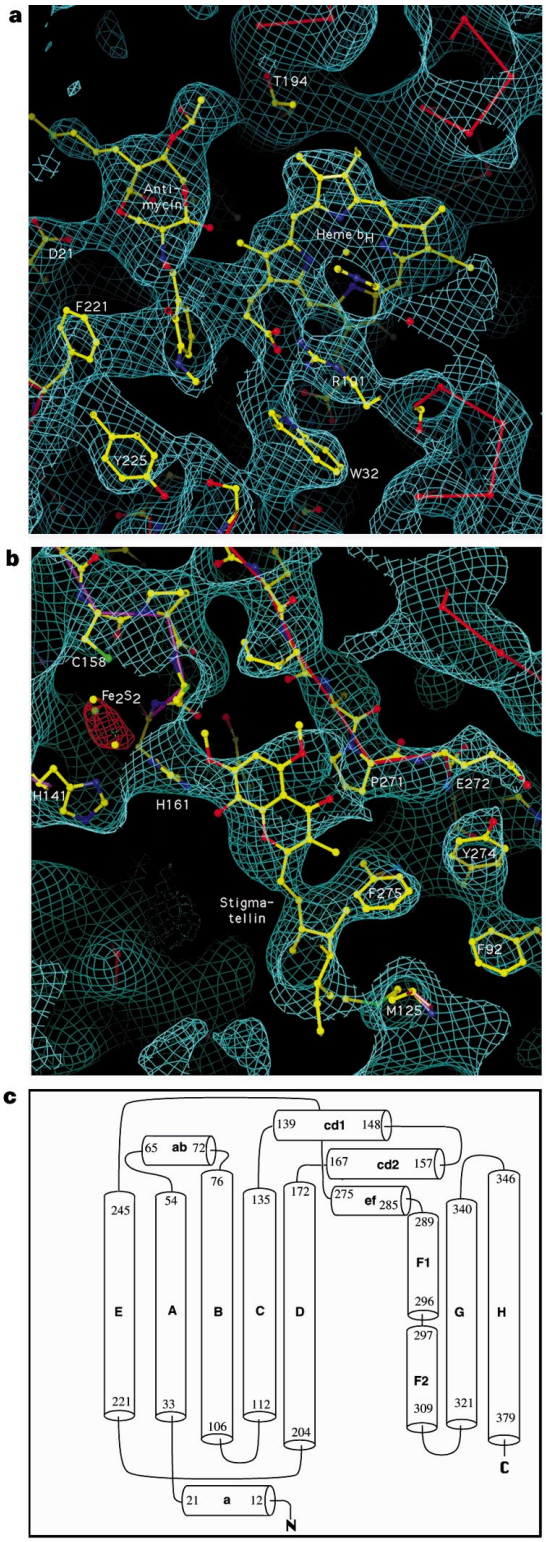

Figure 2 Inhibitor-binding sites. The electron-density maps (**a**, **b**) are from bc_1 crystals containing the inhibitors. **a**, Antimycin-binding site; electron-density map contoured at 0.7 σ. **b**, Stigmatellin-binding site; density contoured at 0.8 (blue) and 5.0 (orange) for the iron–sulphur cluster. The backbone of cytochrome *b* is in red and that of the iron–sulphur protein is in magenta. **c**, Schematic drawing of the secondary structure of cytochrome *b*. Given the number of a residue in the chicken sequence (used here), the number of the corresponding residue in the *Sacharomyces cerevisiae* sequence (conventionally used for alignment) is found by subtracting 2 if the number is less than 114. For residues 114 and later, the numbering is the same as in yeast. The number of the corresponding residue in the beef sequence is found by subtracting 1 from the number in the chicken sequence after the first five residues.

moved from its position in the native crystal (see below), are near the inhibitor. Residues 126–129 of helix C, and 140–147 of the linker cd, are also close by. In the native crystals, Y279 passes through the region at which we have modelled the stigmatellin head group, but in the stigmatellin-bound crystal Y279 has moved and interacts with R283 and with the Rieske backbone around C160. The electron density that we attribute to stigmatellin is strongly connected to the Rieske protein at the position of H161. This may represent a hydrogen bond responsible for holding the Rieske protein in its proximal position (see below) in the presence of myxothiazol. Formation of such a hydrogen bond between stigmatellin[20] or ubiquinol[21,22] at the Q_o site and a Rieske cluster histidine has been previously suggested.

The myxothiazol site. Myxothiazol (not shown) binds in roughly the same place as stigmatellin, but is displaced slightly towards the centre of the membrane and the low-potential *b* haem group (b_L). It is also close to P271, but whereas stigmatellin reaches outward from P271 toward the Rieske protein, myxothiazol and MOA-stilbene reach toward Y132 and F129 in helix C, in the vicinity of b_L. This may be the site from which electron transfer from the ubisemiquinone to the cytochrome b_L haem occurs.

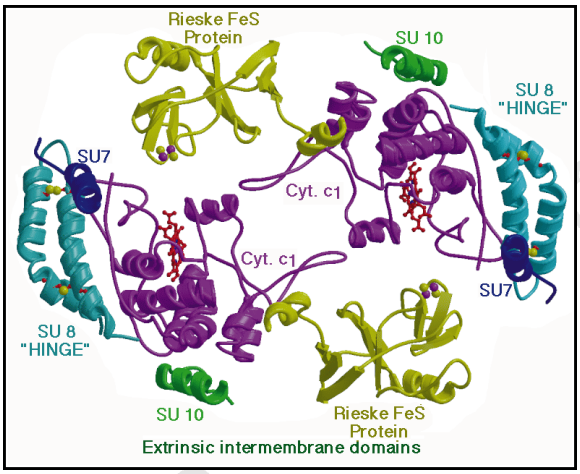

Figure 3 Structure of the intermembrane (external surface) domains of the chicken bc_1 complex. This is viewed from within the membrane, with the transmembrane helices truncated at roughly the membrane surface. Ball-and-stick models represent the haem group of cytochrome c_1, the Rieske iron–sulphur cluster, and the disulphide cysteines of subunit 8. SU, subunit; cyt, cytochrome.

Table 2 Distances between the Rieske iron–sulphur cluster and cytochromes c_1 and b_L

Crystal	Distance (Å) from Fe_2S_2 cluster to		Designation (proximal/distal from haem b_L)
	Haem b_L	Haem c_L	
Beef $P4_122$ (from ref. 12)	27.0	31.0	Proximal
Chicken $P2_12_12_1$ (+stigmatellin)	26.4	31.6	Proximal
Chicken $P2_12_12_1$	34.3	21.3	Distal
Beef $P6_522$	34.9	17.2	Distal
Beef $P2_1$	35.1	17.5	Distal
Rabbit $P6_522$	35.5	19.1	Distal

Iron peaks were located as peaks in electron density, calculated from averaged experimental phases and improved and extended by molecualr averaging, except for chicken $P2_12_12_1$ in the absence of inhibitor, in which case Bivoet difference amplitudes were used with improved experimental phases retarded by 90°.

Arrangement of the intermembrane protein domains

Figure 3 shows a slab including the extrinsic domains in the intermembrane region of the chicken complex. The two cytochrome c_i molecules contact each other through loops that surround an empty area around the two-fold axis. Subunit 8 (the 'hinge protein for formation of the cytochrome c_1–*c* complex' of ref. 23) and the external ends of subunits 7 and 10 interact with cytochrome c_1 on the side away from the dimer interface. The hinge protein consists of a bent hairpin held by two internal disulphide bonds.

Structure of cytochrome c_1

Cytochrome c_1 is one of the three redox-active proteins in the cytochrome bc_1 complex, but is incomplete in the beef complex structure[12]. The subunit is well ordered in our chicken crystals and the entire polypeptide can be traced. Its extrinsic domain forms a wedge-like structure containing the haem group, with a C-terminal transmembrane anchor next to helix E of cytochrome *b*. Figure 4 compares the backbone-folding patterns of cytochrome c_1 and mitochondrial cytochrome *c*, the prototype of Ambler's class I cytochromes *c*[24]. Cytochrome *c* has five helical segments, α1–α5.

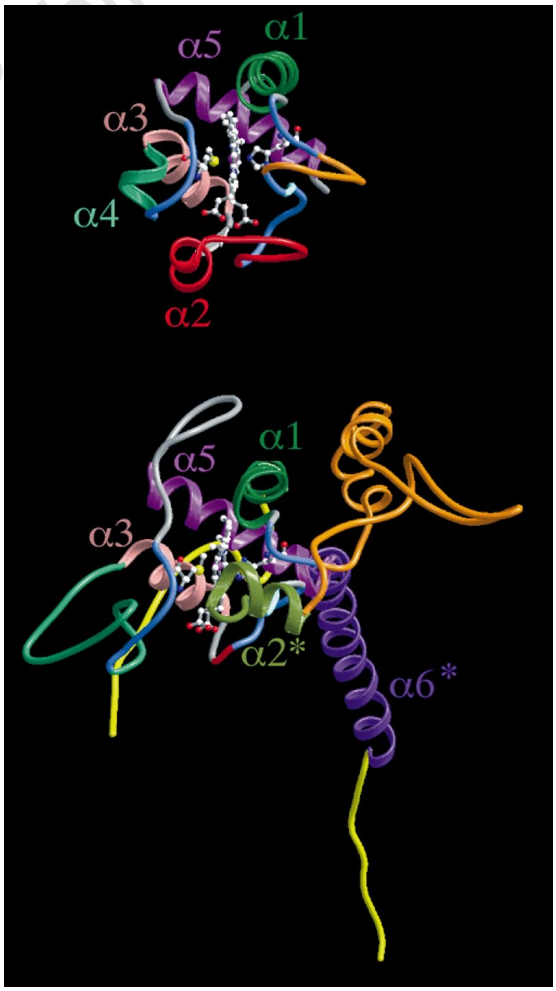

Figure 4 The structures of cytochrome c_1 and cytochrome *c*. Top, the ribbon diagram of mitochondrial cytochrome *c* with the open corner of the C pyrrole of the haem group facing the viewer, and the haem propionates directed downwards. Bottom, our current structure of cytochrome c_1, rotated to put the common features between the two cytochromes in the same orientation. Corresponding segments of each cytochrome are drawn with the same colour. Helices labelled α1, α3, and α5 correspond to similarly labelled and coloured helices in cytochrome *c*, whereas those labelled α2* and α6* have no counterpart in cytochrome *c*.

Three helices (α1, α3 and α5), which are conserved in class I cytochromes in general, are present in cytochrome c_1 and occupy the same positions relative to each other and to the haem. Conserved aromatic residues involved in interactions between α1 and α5 (F10 and Y97 in mitochondrial cytochrome) are present as Y33 and F189, respectively. The tripeptide PNL, starting at residue 30, is conserved in mitochondrial cytochromes *c*. The proline carbonyl accepts a hydrogen bond from N^{δ} of the histidine haem ligand and the leucine provides a hydrophobic environment for the haem ring. This aligns with the tripeptide PDL that begins at residue 111 of cytochrome c_1. It is conserved in all cytochromes c_1 except that of *Rhodobacter sphaeroides*, which, barring a sequencing error, has the tripeptide ADL. These similarities justify inclusion of cytochrome c_1 as a class I cytochrome.

In mitochondrial cytochromes *c* the pyrrole C corner of the haem group is exposed at the 'front' face, where electron transfer is thought to take place. This corner is also exposed in our cytochrome c_1 structure. The exposed C corner of the haem is surrounded by three regions of the protein, consisting of residues 36–41 (corresponding to cytochrome *c* 13–18, 'fingerprint' region), the side chain of Y95 and residues 104–106 (helix 2′; no corresponding residues in cytochrome c), and residues 158–163 (containing the haem ligand M160 and corresponding to cytochrome *c* residues 77–82).

Major differences between cytochromes *c* and c_1 are the result of insertions or deletions in loop regions. For example, bovine cytochrome c_1 has an N-terminal extension of 24 residues before helix α1, whereas bovine cytochrome *c* has a one-residue extension. In cytochrome c_1 this extension interacts with subunit 8, the hinge protein. After helix α1 and the 'fingerprint' haem-binding stretch, CXXCH which are similar in the two cytochromes, cytochrome c_1 has a long insertion (residues 42–109 of cytochrome c_1 replace residues 18–28 of cytochrome *c*). This expanded loop includes a region implicated in cytochrome *c* binding[25] and the dimer contact with cytochrome c_1 in the other monomer seen in Fig. 3. Another insertion is found between the methionine haem ligand and helix 5; the six residues 81–86 in cytochrome *c* correspond to eighteen residues (161–178) in the c_1 cytochromes. This region has also been implicated in cytochrome *c* binding[26]. The end of helix α5 is the C terminus of cytochrome *c* but the transmembrane helix α6′ is found after α5 cytochrome c_1.

There is a second exposure of the haem on the A–D edge: the long loop present in cytochromes *c* and c_2, corresponding to residues 41–58 in tuna cytochrome *c*, is absent in cytochrome c_1. This results in exposure of the haem propionates to the surface. As described below, this edge is within electron-transfer distance of the iron–sulphur cluster in some crystals, indicating that this may be the pathway for reduction by the iron–sulphur protein.

The Rieske iron–sulphur protein

Another of the three functionally important redox-active subunits of the cytochrome bc_1 complex, the Rieske iron–sulphur protein, is missing in the structure of the tetragonal beef crystal[12]. Electron densities in the region of the globular extrinsic domain of this protein in our crystals are weaker than those in the rest of the structure, but are present and recognizable (Fig. 5). The backbone density is completely connected only when contoured at 1 σ or lower, whereas the cytochrome *b* backbone in the transmembrane helices was continuous even when contoured at 3 σ. However, the density was good enough to unambiguously locate the known structure of the soluble domain of the Rieske protein[27].

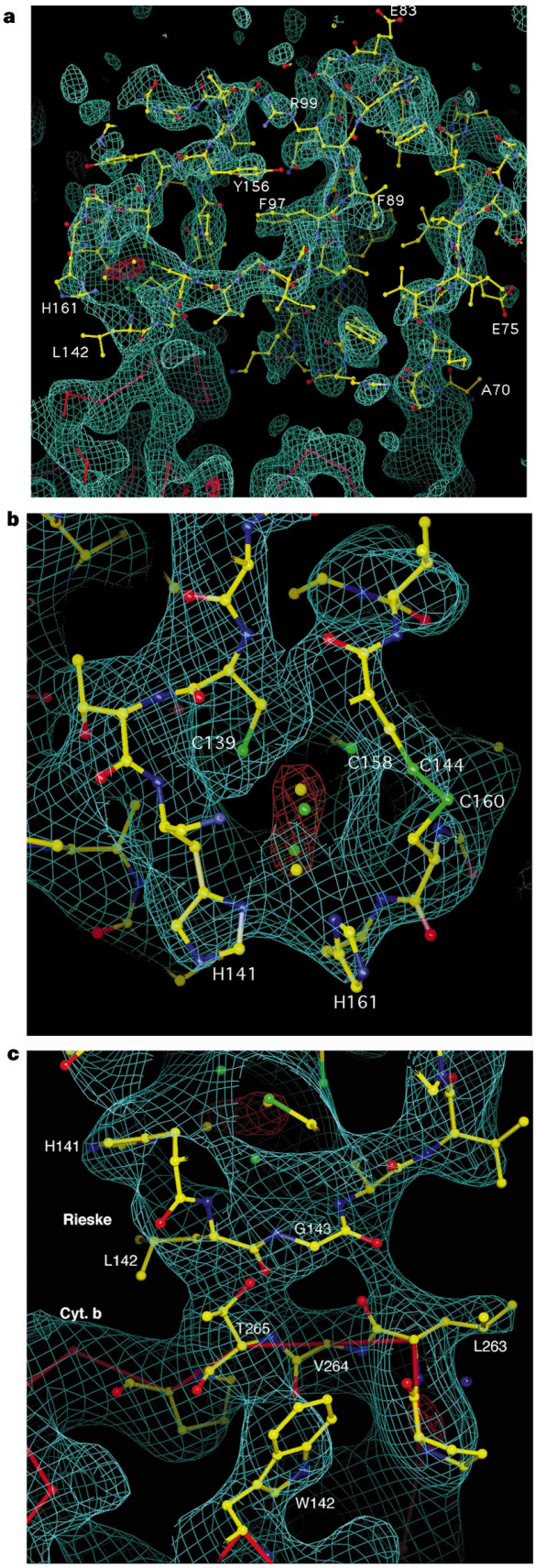

◀ **Figure 5** The Rieske iron–sulphur protein. The electron-density maps are from improved experimental phases, contoured at 1 σ (blue) and 5 σ (red). The atomic model of the soluble domain of the iron–sulphur protein is from the coordinates of the protein database entry 1RIE (ref. 27), positioned as described in the text. **a**, A slab through the protein, including the iron–sulphur cluster (orange net) and the connection to the transmembrane helix (around residue 70). **b**, A close-up view of the electron density around the iron–sulphur cluster (orange net) of the Rieske protein. **c**, Contact of the Rieske protein (in the haem *b* distal conformation) with cytochrome (cyt) *b*. The model of cytochrome *b* (red Cα backbone plus ball-and-stick models for residues W142 and L263 to P266) is from our coordinates.

As predicted from hydropathy plots and molecular-engineering results[28,29], the iron–sulphur protein has a membrane-spanning helical segment near the N terminus. This was removed by proteolysis in preparing the soluble domain for structure determination[27]. In our electron-density map (Fig. 5a), the electron density continues before residue 70 where the model starts, and connects to a transmembrane helix. The transmembrane helix is well ordered.

The N-terminal 24 residues are on the matrix side, and interact with subunit 1. Residues 25–62 form a transmembrane helix, and are close to the transmembrane helices of subunit 10 and cytochrome c_1 (and, in the mammalian crystals, the putative subunit 11). The transmembrane helix is slightly curved and highly slanted. It passes through the membrane at an angle of about 32° to the two-fold axis, which is assumed to be perpendicular to the membrane. This high degree of tilt accounts for the length of the transmembrane helix (37 residues), which previously led to suggestions of two transmembrane helices for the Rieske protein[29].

Residues 60–66 are in close contact with both cytochrome *b* subunits in the dimer, whereas residues 67–73 provide a flexible 'tether' connecting the extrinsic domain of the Rieske protein to its transmembrane helix. Figure 5b shows a close-up view of the iron–sulphur cluster region of the Rieske protein. Two histidine ligands, residues 141 and 161, are seen as bulges in the density at the tip of the protein. The iron atoms (orange net) are not individually resolved in this map.

Swapping of extrinsic domain between monomers

Except for the transmembrane helix, only residues 141–143 of the iron–sulphur protein (one of the two loops that enclose the iron–sulphur cluster) contact with cytochrome *b* in the native chicken crystals. This contact (Fig. 5c) seems to involve interaction of residues L142 and G143 of the Rieske protein of one monomer with T265 and L263 of cytochrome *b* of the other monomer.

The extrinsic domain of the iron–sulphur protein has no contacts with the other extrinsic domains within a monomer in the native chicken crystals (Fig. 3). But the iron–sulphur cluster is close to the haem group of cytochrome c_1 of the other monomer within the complex dimer. As described below, this may provide the pathway for electron transfer between the iron–sulphur protein and cytochrome c_1. Taking monomers to be as defined above, the iron–sulphur cluster of one monomer is in a position to transfer electrons with cytochromes *b* and c_1 of the other monomer.

The small number of contacts with the rest of the dimer probably accounts for the poor order of the Rieske extrinsic domain, and indicates that the domain may be mobile (also suggested in ref. 12). This mobility is restricted in one monomer of the chicken crystals, and in the beef and rabbit hexagonal crystals, by interdimeric crystal contacts involving the extrinsic domain of the Rieske protein. The poor order of the extrinsic domain in the beef crystals and the large distance between the cluster and the haem of cytochrome c_1 indicated that this mobility may be required for function (ref. 12).

Two conformations of the Rieske protein

Although the distances between the six haem-iron peaks of the dimer were the same (within experimental error) in all four crystal forms, the distance from the iron–sulphur cluster to any haem group varied by up to 5 Å in the different native crystals. From published distances between iron centres, it is clear that iron–sulphur clusters in the tetragonal beef crystals[11,12] and in any of our native crystals are positioned differently (Table 2). But when we treated the chicken cytochrome bc_1 complex with a saturating amount of stigmatellin before crystallization, the extrinsic domain of the iron–sulphur protein was found at a location different to that in native crystals, and the iron–sulphur cluster was in the same position as in the tetragonal beef[12] crystals. This movement can be simply and dramatically demonstrated using Bivoet difference maps constructed from diffraction data collected with X-ray wavelength near the iron absorption edge. Because of anomalous scattering by iron, the peaks in such maps indicate positions of irons in the complex: the three haem irons of the cytochromes and the iron–sulphur cluster of the Rieske protein. Bivoet difference maps are shown in Fig. 6. The peaks labelled Fe–S move closer to the haem groups of cytochrome *b* in the presence of stigmatellin. We call this the proximal conformation of the Rieske protein; the conformation in our native crystals is the distal conformation. The relative position of the iron–sulphur cluster in the chicken crystals containing stigmatellin is 16 Å from the position in the native chicken crystals, and 20 Å from that in the beef hexagonal crystals.

Stereo views of the two conformations of the Rieske protein, in the context of the entire bc_1 complex dimer and in isolation with cytochrome *b* and the haem of cytochrome c_1, are shown in Fig. 1b, c. The two locations of the extrinsic domain of the Rieske protein are related by a rotation of 57° about an axis passing near residues 93 and 182 of the protein, perpendicular to the plane of the picture in Fig. 1c. The transmembrane helix and matrix-side portion are unchanged in the presence of stigmatellin. The coil consisting of residues 68–73 is stretched out in the presence of stigmatellin, allowing this end of the soluble domain to move farther from the membrane as the Fe_2S_2 cluster on the other end moves closer. In a crystal containing bound stigmatellin and antimycin, the position of the iron–sulphur cluster was nearly the same as in the stigmatellin-bound crystal. In crystals containing only antimycin or

Table 3 Structure-determination statistics: diffraction data for chicken bc_1 crystals

	d_{min}	Number of reflections	Unique reflections	Completeness (%) ($I > 1\sigma$)	R_{merge} (%)	X-ray source*
Native						
chn21	3.60	279,119	70,363	76.3 (58.1)	18.6	RA
chc01	3.10	556,456	123,869	91.6 (80.5)	10.2	SSRL
chm	3.01	569,255	141,427	96.6 (74.2)	16.2	SSRL
chb	2.95	433,902	131,641	81.7 (51.2)	27.8	BNL
Derivative						
PIP†	3.50	292,339	86,221	91.8 (76.3)	10.8	SSRL
NSDMA‡	3.90	425,028	67,109	99.7 (79.0)	12.4	RA
TML02§	3.50	203,105	61,380	65.2 (53.5)	17.1	RA
TML03§	4.30	110,201	38,103	74.4 (50.6)	21.6	RA
HPDL¶	4.00	129,187	48,715	78.4 (54.0)	20.2	RA
Iridium‖	3.50	177,303	68,522	71.7 (43.5)	13.4	RA
TMLssrl§	3.50	160,826	61,128	65.6 (43.9)	19.9	SSRL
HPDLssrl¶	3.15	350,204	93,367	71.6 (60.2)	19.3	SSRL

Each line corresponds to one data set collected from a single native or derivatized crystal of chicken cytochrome bc_1.
* X-ray sources and wavelengths are indicated by: RA, rotating anode (1.54 Å); SSRL, Stanford Synchrotron Radiation Laboratory BL7-1 (1.08 Å); BNL, Brookhaven National Laboratory X-12b (1.006 Å).
† Ethylenediamine platinum iodide$_2$.
‡ *N*-(5-nitrosalicyl)-(*S*-decylmercuri)6-aminothiophenol, a putative antimycin analogue.
§ Trimethyl lead acetate (different concentrations and soaking times).
¶ Hexaphenyl di-lead.
‖ Iridium carbonyl.

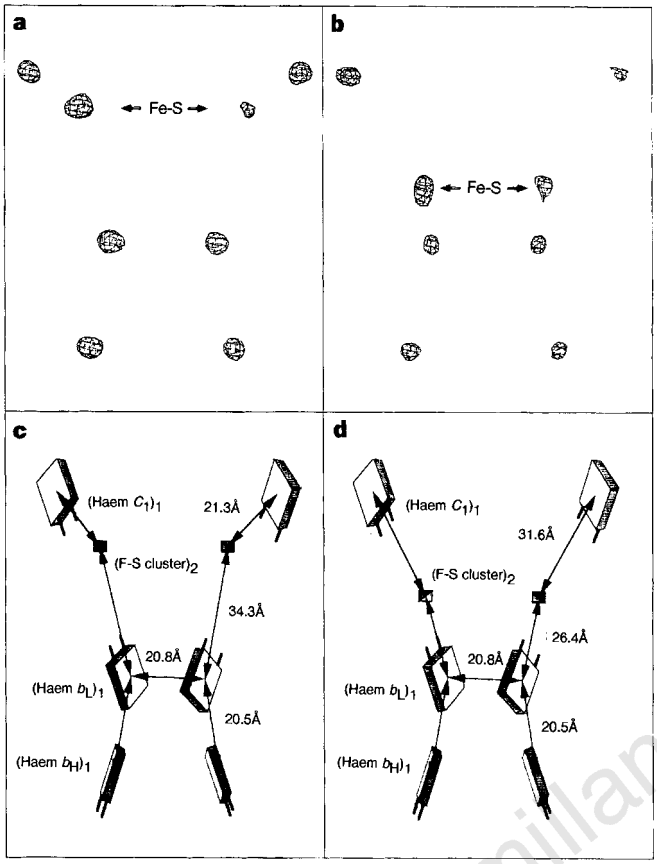

Figure 6 Relative positions of the redox centres in the two different conformations of the bc_1 complex dimer. **a**, **b**, Iron centres revealed by anomalous scattering near the iron edge. The net is a Bivoet difference map with X-ray wavelength 7,131 eV phased with experimental phases improved by averaging, and contoured at 4.5 σ. **c**, **d**, Schematic drawing representing the cofactors. **a**, **c**, Results from a native crystal, with the iron–sulphur cluster of the Rieske protein in the distal position (from the low-potential haem group of cytochrome *b*). **b**, **d**, Results from a crystal containing bound stigmatellin, with the cluster in the proximal position.

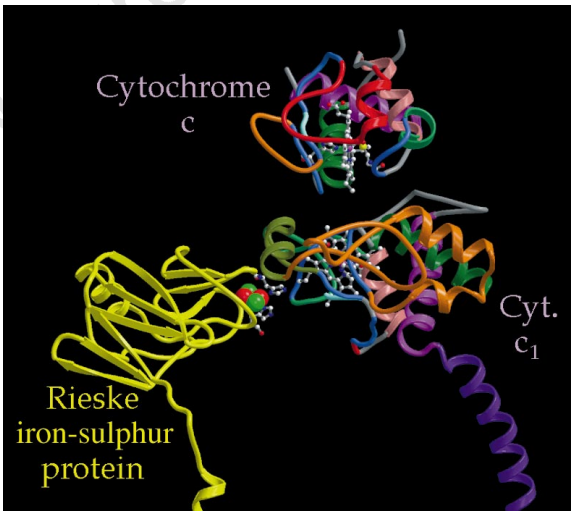

Figure 7 Electron pathway through cytochrome c_1 in a hypothetical complex of the bc_1 complex with cytochrome *c*. The ribbon diagram shows the backbones of cytochrome c_1, cytochrome *c* (both with the same colour scheme as in Fig. 4) and the Rieske protein (yellow). The haem groups, the iron–sulphur cluster and surrounding residues are drawn as ball-and-stick models. The balls representing the iron–sulphur cluster (red and green) are enlarged for visibility. The position of the Rieske protein relative to cytochrome c_1 is obtained from our beef hexagonal crystals.

myxothiazol, position of the iron–sulphur cluster was similar to that in the crystals without inhibitors.

In the proximal conformation, the iron–sulphur cluster ligand H161 of the Rieske protein is in H-bond distance of the occupant of the Q_o site (stigmatellin in our crystals (Fig. 2b), but, by inference, the electron donor ubiquinol *in vivo*), and in the distal conformation the iron–sulphur cluster is close to its electron acceptor, the haem group of cytochrome c_1. This suggests that the reaction mechanism for electron transfer in the cytochrome bc_1 complex requires this dramatic conformational change, involving movement of the extrinsic domain of the iron–sulphur protein.

Electron transfer to cytochrome c_1

In the native chicken crystals, the second loop of the Rieske protein enclosing the cluster (residues around H161) faces toward cytochrome c_1, approaching the haem propionates and residues 106 and 145 of cytochrome c_1 (Fig. 3). As shown in Table 2, the Rieske protein is closer to cytochrome c_1 in our two beef crystals. In these crystals there is electron-density contact at the 2 σ level, between the Rieske protein around C160 (which forms a disulphide bond holding the cluster-binding loops together) and cytochrome c_1 around G107 (between helix $\alpha 2'$ and the haem-bracing P111). This electron density probably represents the configuration of the iron–sulphur protein during electron transfer to the cytochrome. Residue H161 of the Rieske protein provides one of the ligands to the Fe_2S_2 cluster, and is 4.0 Å from an oxygen atom of haem propionate D and 8.2 Å from the edge of the haem π-bonded system at the C3D atom. From this distance (8.2 Å) we can calculate a rough rate of electron transfer from the iron–sulphur protein to cytochrome c_1 of 4.8–80 $\times$ 10^6 s^{-1}, assuming nonadiabatic electron tunnelling with reorganization energy of 0.7–1.0 electron volts and ΔG° near zero[30,31]. This is significantly faster than estimated rates for this reaction[32] so if the protein spends a small fraction of time in this conformation it could account for the reaction rate. In the native chicken crystals, this distance is 14.4 Å, which would give a rate of 1.8–15 $\times$ 10^3 s^{-1}) with the same assumptions. In the crystal containing stigmatellin, or the tetragonal beef crystals[12], the shortest distance from the cluster or its ligands to the haem tetrapyrrole ring is 27 Å, giving (with the same assumptions) a rate of 10^{-4} s^{-1} and making it very unlikely that the enzyme could function in this single conformation.

Model for electron transfer

Figure 7 shows a ribbon diagram of the extrinsic domains of the Rieske iron–sulphur protein and cytochrome c_1, as well as of cytochrome *c* bound to cytochrome c_1 at a hypothetical site and orientation. The position of the iron–sulphur protein is that obtained from the beef $P6_522$ crystals. This diagram illustrates the possibility of electron transfer into cytochrome c_1 through the D propionate and out of cytochrome c_1 through the C corner of the haem to cytochrome *c*. The distance between the two cytochromes is 10.2 Å, measured between atoms C2C of each haem group (the closest approach of the π-bonded systems). Assuming ΔG° near zero and reorganization energy λ in the range 0.7–1.0 gives electron-transfer rates in the range of 0.6–5.1 $\times$ 10^6 s^{-1}. □

Methods

Purification and crystallization. The cytochrome bc_1 complex was purified from different vertebrate heart tissues nearly as described for the potato complex[33]. Mitochondria were prepared as described[34] and were solubilized using the detergent dodecyl maltoside. We isolated the complex from the extract by chromatography on DEAE Sepharose CL6B and further purified by size-exclusion chromatography on Sepharose CL6B[13]. The protein was concentrated to ~200 μM by ultrafiltration through an Amicon YM-100 membrane, precrystallized by mixing with 100 mM KMES pH 6.5 and 10% PEG-4000, and redissolved in 20 mM K-MOPS 7.5, 20 g l^{-1} *n*-octyl-β-D-glucopyranoside and 100 mM NaCl. Aliquots (5–20 μl) were mixed with an equal

volume of precipitant containing 20 mM KMES pH 6.7, 75 mM NaCl, 10% glycerol, and 6% PEG-4000, and were subjected to vapour diffusion against 30% glycerol.

To cocrystallize the bc_1 complex with the high-affinity inhibitors antimycin, myxothiazol, and stigmatellin, we added inhibitor from an ethanolic solution (the final ethanol concentration was below 1% v/v) in a 1.5–2.0-fold molar ratio to the pooled fractions from the final column at a protein concentration of 5–10 μM, before concentration and precrystallization as above.

Cryogenic-data collection and reduction. After crystallization was complete (5–30 days after setup), we added 20 μl cryoprotectant containing 10 mM K-MES pH 6.7, 10 mM *n*-octyl-β-D-glucopyranoside, 25% glycerol and 10% PEG-4000 to the solution containing the crystals from chicken complex, and changed the reservoir to 35% glycerol for further concentration of glycerol and PEG without increasing ionic strength. After this equilibration, or, in some cases, after further soaking in cryoprotectant consisting of 30% glycerol, K-MES and *n*-octyl-β-D-glucopyranoside, crystals were frozen in liquid ethane or nitrogen, or in the cryogenic stream, and data were collected at 70–100K. A suitable procedure for flash-freezing the beef and rabbit crystals has not yet been developed. We processed diffraction data by the programs DENZO and SCALEPACK[35].

Structure determination. Data-collection statistics are summarized in Table 3. The chicken crystals were phased by isomorphous replacement and the resulting electron density was used to phase the other crystal forms by molecular replacement. Heavy-atom derivatives were first analysed using XtalView[36]. We used the RAVE package[37] for molecular averaging, map skewing, and rotation-translation-operator improvement. We used the CCP4 package[38] for final heavy-atom refinement and phase calculation (program MLPHARE) and for finding molecular replacement solutions (programs ALMN and TFFC). The phases were improved and extended to the resolution limit of the data by multicrystal and non-crystallographic symmetry averaging. During the phase improvement and extension process, correlation coefficients between the calculated electron-density map of the Rieske protein and our experimental electron density, monitored as a measure of the improvement of the maps, increased to 80–85% in the different data sets. The coefficient between subunits 1 and 2 increased to 40–48%.

Model building was done with the program O (ref. 39) and structures illustrated using this program or Molscript[40] and Raster3D (ref. 41).

All subunits of the bc_1 complexes of vertebrates are expressed in the cytoplasm, except cytochrome *b*. Cytochrome *b*, which is expressed in mitochondria, has sequence identity of 74% between chicken and cows. As amino-acid sequences of the cytoplasmically expressed chicken subunits of the complex have not been reported, we used the sequences of the beef proteins for model building. Cytochrome *c*, a cytoplasmically expressed mitochondrial protein, has 89.5% identity between chicken and cows. Myosin light chain II of chicken is 91% identical to the human or mouse proteins.

Location of iron centres from anomalous data. Anomalous data at wavelength near the iron K absorption edge (7,131 eV) were collected for native and stigmatellin-containing crystals. Bivoet difference maps were made with coefficients of $(F^+ - F^-)$ and improved experimental phases retarded by 90° to locate the iron centres.

Electron density map calculations. The electron-density maps were calculated using coefficients of $(2F_o - F_c)e^{-i\Phi_c}$, where the F_o values are from the experimentally determined intensities but the F_c and Φ_c values are calculated from the previous map after multiple-crystal averaging. In the case of unobserved reflections, F_o was replaced by F_c as recommended[42], resulting in coefficients of $F_c e^{-\Phi_c}$ for those terms. This 'fill-in' procedure was used both during averaging and, unless otherwise noted, in making the final maps used in the figures.

Received 12 December 1997; accepted 20 February 1998.

1. Mitchell, P. Coupling of phosphorylatin to electron and proton transfer by a chemiosmotic type of mechanism. *Nature* **191,** 144–148 (1961).
2. Hinkle, P. C., Kumar, M. A., Resetar, A. & Harris, D. L. Mechanistic stoichiometry of mitochondrial oxidative phosphorylation. *Biochemistry* **30,** 3576–3582 (1991).
3. Mitchell, P. Possible molecular mechanisms of the protonmotive function of cytochrome systems. *J. Theor. Biol.* **62,** 327–367 (1976).
4. Crofts, A. R. in *The Enzymes of Biological Membranes*, Vol. 4 (ed. Martonosi, A. N.) 347–382 (Plenum, New York, 1985).
5. Schägger, H., Link, T. A., Engel, W. D. & von Jagow, G. Isolation of the eleven protein subunits of the bc_1 complex from beef heart. *Methods Enzymol.* **126,** 224–237 (1986).
6. Schaegger, H., Brandt, U., Gencic, S. & von Jagow, G. Ubiquinol-cytochrome-c reductase from human and bovine mifochondria. *Methods Enzymol.* **260,** 82–96 (1995).
7. Weiss, H. & Leonard, K. Structure and function of mitochondrial ubiquinol:cytochrome c reductase and NADH:ubiquinone reductase. *Chemica Scripta* **27B,** 73–81 (1987).
8. Yue, W. H., Zou, Y. P., Yu, L. & Yu, C. A. Crystallization of mitochondrial ubiquinol-cytochrome c reductase. *Biochemistry* **30,** 2303–2306 (1991).
9. Kubota, T. *et al.* Crystallization and preliminary X-ray crystallographic studies of bovine heart mitochondrial cytochrome bc_1 complex. *J. Mol. Biol.* **221,** 379–382 (1991).
10. Berry, E. A., Huang, L.-S., Earnest, T. N. & Jap, B. K. X-ray diffraction by crystals of beef heart ubiquinol:cytochrome c oxidoreductase. *J. Mol. Biol.* **224,** 1161–1166 (1992).
11. Yu, C.-A. *et al.* Crystallization and preliminary structure of beef heart mitochondrial cytochrome-bc_1 complex. *Biochim. Biophys. Acta* **1275,** 47–53 (1996).
12. Xia, D. *et al.* Crystal structure of the cytochrome bc_1 complex from bovine heart mitochondria. *Science* **277,** 60–66 (1997).
13. Berry, E. A., Huang, L.-S., Shulmeister, V. M. & Kim, S.-H. A new form of crystal of bovine heart ubiquinol:cytochrome c oxidoreductase—determination of space group and unit cell parameters. *Acta Crystallogr. D* **51,** 235–239 (1995).
14. Crofts, A. R. *et al.* in *The Phototrophic Prokaryotes—Proceedings of the IXth Int. Symp. on Phototrophic Prokaryotes, Vienna, Sept. 1997)* (eds Peschek, G. A., Loeffelhardt, W. & Schmetterer, G.) (Plenum, New York, London, Washington DC, Boston, in the press).
15. Brandt, U., Yu, L., Yu, C. A. & Trumpower, B. L. The mitochondrial targeting presequence of the Rieske iron-sulfur protein is processed in a single step after insertion into the cytochrome bc_1 complex in mammals and retained as a subunit in the complex. *J. Biol. Chem.* **268,** 8387–8390 (1993).
16. Beautement, K., Clough, J. M., Defraine, P. J. & Godfrey, C. R. A. Fungicidal beta-methoxyacrylates—from natural products to novel synthetic agricultural fungicides. *Pestic. Sci.* **31,** 499–519 (1991).
17. Clough, J. M. & Godfrey, C. R. A. Growing hopes. *Chemistry In Britain* **31,** 466–469 (1995).
18. Sauter, H., Ammermann, E. & Roehl, F. in *Crop Protection Agents from Nature* (ed. Copping, L. G.) 50–81 (Royal Soc. Chem., Thomas Graham House, Cambridge, UK, 1996).
19. Slater, E. C. The mechanism of action of the respiratory inhibitor, antimycin. *Biochim. Biophys. Acta* **301,** 129–154 (1973).
20. Link, T. A. in *Frontiers of Cellular Bioenergetics: Molecular Biology, Biochemistry and Physiopathology* (eds Papa, S., Guerrieri, F. & Tager, J. M.) (Plenum, New York, London, in the press).
21. Robertson, D. E., Daldal, F. & Dutton, P. L. Mutants of ubiquinol-cytochrome c2 oxidoreductase resistant to Qo site inhibitors: consequences for ubiquinone and ubiquinol affinity and catalysis. *Biochemistry* **29,** 11249–11260 (1990).
22. Link, T. A. The role of the "Rieske" iron sulfur protein in the hydroquinone oxidation (Qp-) site of the cytochrome bc1 complex: the "proton-gated affinity change" mechanism. *FEBS Lett.* **412,** 257–264 (1997).
23. Kim, C. H. & King, T. E. A mitochondrial protein essential for the formation of the cytochrome c_1-c complex. Isolation, purification, and properties. *J. Biol. Chem.* **258,** 13543–13551 (1983).
24. Ambler, R. P. Sequence variability in bacterial cytochromes c. *Biochim. Biophys. Acta* **1058,** 42–47 (1991).
25. Stonehuerner, J. *et al.* Identification of the binding site on cytochrome c_1 for cytochrome c. *J. Biol. Chem.* **260,** 5392–5398 (1985).
26. Broger, C., Salardi, S. & Azzi, A. Interaction between isolated cytochrome c_1 and cytochrome c. *Eur. J. Biochem.* **131,** 349–352 (1983).
27. Iwata, S., Saynovits, M., Link, T. A. & Michel, H. Structure of a water soluble fragment of the 'Rieske' iron-sulfur protein of the bovine heart mitochondrial cytochrome bc_1 complex determined by MAD phasing at 1.5 Å resolution. *Structure* **4,** 567–579 (1996).
28. Van Doren, S. R., Yun, C.-H., Crofts, A. R. & Gennis, R. Assembly of the Rieske iron-sulfur subunit of the cytochrome bc_1 complex in *Escherichia coli* and *Rhodobacter sphaeroides* membranes independent of the cytochrome b and c_1 subunits. *Biochemistry* **32,** 628–636 (1993).
29. Link, T. A., Schägger, H. & von Jagow, G. in *Cytochrome Systems: Molecular Biology and Bioenergetics* (eds Papa, S., Chance, B. & Ernster, L.) 289–301 (Plenum, New York, 1987).
30. Moser, C. C., Page, C. C., Farid, R. & Dutton, P. L. Biological electron transfer. *J. Bioenerg. Biomembr.* **27,** 263–274 (1995).
31. Ding, H. *et al.* Ubiquinone pair in the Q_o site central to the primary energy conserving reactions of cytochrome bc_1 complex. *Biochemistry* **34,** 15979–15996 (1995).
32. Crofts, A. R. & Wang, Z. How rapid are the internal reactions of the ubiquinol:cytochrome c_2 oxidoreductase? *Photosynthesis Res.* **22,** 69–87 (1989).
33. Berry, E. A., Huang, L.-S. & DeRose, V. Ubiquinol-cytochrome c oxidoreductase of higher plants. Isolation and characterization of the bc_1 complex from potato tuber mitochondria. *J. Biol. Chem.* **266,** 9064–9077 (1991).
34. Smith, A. L. Preparation, properties, and conditions for assay of mitochondria: slaughterhouse material, small scale. *Methods Enzymol.* **10,** 81–86 (1967).
35. Otwinowski, Z. in *Proceedigns of the CCP4 Study Weekend: "Data Collection and Processing"* (eds Sawyer, L., Isaacs, N. & Bailey, S.) 56–62 (SERC Daresbury Laboratory, UK, 1993).
36. McRee, D. E. A visual protein crystallographic software system for X11/XView. *J. Mol. Graph.* **10,** 44–46 (1992).
37. Jones, T. A. in *Proc. CCP4 Study Weekend, Molecular Replacement* (eds Dodson, E. J., Glover, S. & Wolf, W.) 91–105 (SERC Daresbury Laboratory, UK, 1992).
38. The SERC (UK) Collaborative Computing Project No. 4. The CCP4 Suite: Programs for Protein Crystallography. *Acta Crystallogr. D* **50,** 760–763 (1995).
39. Jones, T. A., Zou, J. Y., Cowan, S. W. & Kjeldgaard, M. Improved methods for building protein models in electron density maps and the location of errors in these models. *Acta Crystallogr. A* **47,** 110–119 (1991).
40. Kraulis, P. J. MOLSCRIPT: a program to produce both detailed and schematic plots of protein structures. *J. Appl. Crystallogr.* **24,** 946–950 (1991).
41. Merritt, E. A. & Murphy, M. E. P. Raster3D version 2.0—a program for photorealistic molecular graphics. *Acta Crystallogr. D* **50,** 869–873 (1994).
42. Rayment, I. Molecular relacement method at low resolution: optimum strategy and intrinsic limitations as determined by calculations on icosahedral virus models. *Acta Crystallogr. A* **39,** 102–116 (1983).

Acknowledgements. We thank T. Link and his co-workers for providing coordinates for the soluble domain of the Rieske iron–sulphur protein before the release from the Protein Data Bank; H. Bellamy for performing the XAFS scan and for advice on MAD data collection; S. Hong for preparing coordinate files for the inhibitors; T. Meyer for critically reading the manuscript; and L. Tong for advice on molecular averaging. This work was supported by the NIH (grants to E.A.B. and A.R.C.) and by the Office of Biosciences and Environmental Research, US Department of Energy (grant to S.-H.K.). The work was partially done at SSRL which is operated by the Department of Energy, Division of Chemical/Material Sciences. The SSRL Biotechnology Program is supported by the NIH Biomedical Resource Technology Program, Division of Research Resources.

Correspondence and requests for materials should be addressed to E.A.B. and S.-H.K. Atomic coordinates of the chicken bc_1 complex have been deposited in the Brookhaven Protein Database for release in May 1998 (accession number 1BCC for the native chicken structure and 3BCC for the stigmatellin+antimycin-inhibited chicken structure).